Two-phase gas-liquid flow in concentric and fully eccentric annuli. Part II: Model development, flow regime transition algorithm and pressure gradient

Roberto Ibarra[a,*], Jan Nossen[b], Murat Tutkun[c]

Institute for Energy Technology (IFE), Kjeller, Norway, 2007

[a] roberto.jose.ibarra-hernandez@ife.no

[b] jan.nossen@ife.no

[c] murat.tutkun@ife.no

*Corresponding author

Address: Department of Fluid Flow and Environmental Technology, Institute for Energy Technology, Instituttveien 18, Kjeller, Norway, 2007.

Telephone: +47 63 80 60 00

Keywords

Annulus flow; concentric; fully eccentric; flow regimes; model; flow regime transitions

Abstract

A model has been developed for the prediction of flow regime transitions, liquid holdup and pressure gradient for horizontal and low-inclination upward two-phase gas-liquid flow in annuli. The model is based on the hydrodynamic behaviour of slug flow and closure relationships developed for full pipe flow, which are adapted to account for the annulus diameter ratio and eccentricity. This includes the improvement of the model for the prediction of the single-phase friction factor in annuli. Model predictions are compared with the experimental data presented in Ibarra *et al.* (2018) and the model shows good agreement for gas-water and gas-oil flow in both concentric and fully eccentric annuli.

1 Introduction

The prediction of flow regime transitions, liquid holdup and pressure gradient in multiphase flows in annuli is critically important for several processes such as well drilling and intervention in long horizontal wells. The development of reliable predictive tools would ensure safer, and more efficient and profitable system design and operations. The experimental data documented in Ibarra *et al.* (2018) constitute a benchmark for developing and validating models, in particular with regard to the up-scaling performance of the models when up-scaled from laboratory to real field conditions.

A detailed literature survey reveals that there exist no flow models which were developed for horizontal or low-inclination two-phase flow in annuli. In this paper, we present our mechanistic approach to predict the transition to dispersed-bubble and slug flow in annuli. The model estimates the total liquid holdup and pressure gradient for both concentric and eccentric annuli. The model predictions are also compared with the experimental data presented in Ibarra *et al.* (2018).

The motivation behind this study is the fact that existing models for flows in annuli have been developed for flow in vertical configurations. These models are also based on conventional pipe data (Taitel *et al.*, 1980; Mishima and Ishii, 1984). This means that they can work and are applicable for two-phase full pipe flows even though they are categorised as flow model for annuli. Kelessidis and Dukler (1989) acquired experimental data on vertical air-water flow for concentric and eccentric annuli and developed a model based on the Taitel *et al.* (1980) approach. They developed the model for concentric annulus and then introduced slight modifications to the model to account for the effect of annulus eccentricity. Using the comparison between the data and the model, they reported that the degree of eccentricity has only minor effect on the flow regime transitions. Caetano *et al.* (1992a, b) developed a mechanistic model for bubble, slug and annular flows in annuli. The model is essentially a two-phase flow model and accounts for the effect of the inner pipe and degree of eccentricity. This hydrodynamic model is found to be predicting the flow regime transitions, liquid holdup and pressure gradient within quantifiable uncertainty bounds.

Additional models for two-phase gas-liquid flows in vertical and inclined annuli can be listed as follows: Hasan and Kabir (1992), Das *et al.* (1999), Sun *et al.* (2004), Yu *et al.* (2010), and Julia and Hibiki (2011).

Rest of the current paper is organised in six sections: Flow regime transition algorithm and the pressure gradient model are presented in Section 2 and Section 3, respectively. Section 4 discusses the sensitivity analysis of the model in terms of liquid holdup and pressure gradient. Section 5 contains the relations required for the closure of the model. Finally, Section 6 presents the main conclusions of this study.

2 Flow Regime Transition Algorithm

Schematic in Figure 1 displays the parameters used for characterising flow regime transitions and slug flow dynamics. The transition from a slug flow to a dispersed-bubble flow can be determined by assuming that the liquid slug accommodates the same fraction of gas as the dispersed-bubble flow at the transition boundary with the same mixture velocity (Barnea and Brauner, 1985; Zhang *et al.*, 2003a). Thus, transition to dispersed-bubble flow occurs when

$$(1 - H_{\mathrm{LS}})U_{\mathrm{M}} > U_{\mathrm{SG}}, \tag{1}$$

where U_{M} is the mixture velocity, U_{SG} is the superficial gas velocity and H_{LS} is the slug liquid holdup which can be estimated using the Gregory *et al.* (1978) correlation,

$$H_{\mathrm{LS}} = \frac{1}{1 + \left(\frac{U_{\mathrm{M}}}{8.66}\right)^{1.39}}. \tag{2}$$

The implementation of the Gregory *et al.* (1978) correlation for the estimation of the slug liquid holdup introduces an empirical approach to the transition criterion to dispersed-bubble flow. The performance of the Zhang *et al.* (2003a) mechanistic model for the estimation of H_{LS} was explored in order to keep the mechanistic approach in the transition criterion. However, it was found that superficial liquid velocities at the transition boundary from the Zhang *et al.* (2003a) model were similar to those obtained using the Gregory *et al.* (1978) correlation, especially at low

U_{SG}. Moreover, there are no H_{LS} models developed for flow in annuli in the literature neither studies to verify the applicability of models developed for full pipe systems.

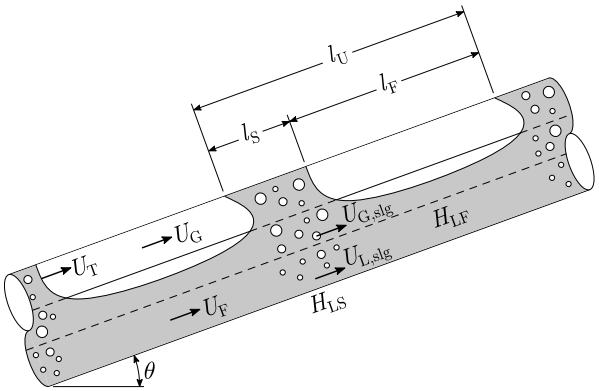

Figure 1: Slug flow model.

Analysis of the slug flow dynamics starts with the continuity equations for fully-developed slugs in a slug unit, l_U. These equations are based on conservation of mass and independent of the annulus configuration. In this formulation we assume no entrainment of liquid droplets in the gas pocket (Taylor bubble), no entrainment of gas bubbles in the liquid film, and no slippage between the liquid and the gas bubbles in the liquid slug (*i.e.* $U_{G,slg} = U_{L,slg} = U_M$). This approach is adapted from the unified model via slug dynamics developed by Zhang *et al.* (2003b) for conventional pipe flow.

The continuity equations for the liquid film and the relation for the slug unit are

$$H_{LS}(U_T - U_M) = H_{LF}(U_T - U_F), \tag{3}$$

$$l_U U_{SL} = l_S H_{LS} U_M + l_F H_{LF} U_F, \tag{4}$$

where U_T is the translational or Taylor bubble velocity, H_{LF} is the liquid holdup in the film region, U_F is the velocity of the liquid film, l_S is the slug length, and l_F is the film length.

Similarly, the continuity equations for the gas phase can be written as:

$$(1 - H_{LS})(U_T - U_M) = (1 - H_{LF})(U_T - U_G), \tag{5}$$

$$l_U U_{SG} = l_S(1 - H_{LS})U_M + l_F(1 - H_{LF})U_G. \tag{6}$$

Equating l_U from Eq. (4) and (6) yields

$$\frac{l_S}{l_F} = \frac{\frac{U_{SG}}{U_{SL}} H_{LF} U_F - (1 - H_{LF}) U_G}{(1 - H_{LS}) U_M - \frac{U_{SG}}{U_{SL}} H_{LS} U_M}. \tag{7}$$

The combined (gas-liquid) momentum equation for the film region (*i.e.* the equation obtained by equating the pressure drop terms in the gas and liquid momentum equation) can be expressed as follows:

$$\frac{\rho_L (U_T - U_F)(U_M - U_F) - \rho_G (U_T - U_G)(U_M - U_G)}{l_F} - \tau_F \frac{S_F}{A_F} + \tau_G \frac{S_G}{A_G} + \tau_i S_i \left(\frac{1}{A_F} + \frac{1}{A_G} \right) - (\rho_L - \rho_G) g \sin\theta = 0, \tag{8}$$

where g is the gravitational acceleration, τ is the shear stress, A is the cross-sectional area, S is the perimeter for: (G) gas phase, (F) film or liquid phase, and (i) gas-liquid interface. The cross-sectional area of the liquid (film) and gas phase are defined as $A_F = H_{LF} A_P$ and $A_G = (1 - H_{LF}) A_P$, respectively, where A_P represents the cross-sectional area of the annulus pipe. The first term on the L.H.S. of Eq. (8) corresponds to the momentum exchange between the slug region and the film region, which is key in the determination of the film velocity and holdup for the slug flow modelling.

At the transition from slug flow to separated flows (*e.g.* stratified), the film length becomes infinitely long ($l_F \to \infty$). Firstly, Eq. (7) along with Eqs. (3) and (5) are used to obtain the liquid film holdup from the continuity relations through the slug unit, H_{LF}, resulting in

$$H_{LF} = \frac{H_{LS}(U_T - U_M) + U_{SL}}{U_T}. \tag{9}$$

Secondly, the combined momentum equation (Eq. (8)), in which the momentum exchange term disappears, is solved to obtain the liquid holdup when $l_F \to \infty$, denoted by $H_{LF(l_F \to \infty)}$. Finally, the transition to slug flow is defined using the minimum slip criterion, which states that at the transition boundary $H_{LF} = H_{LF(l_F \to \infty)}$. Figure 2 shows the flow chart used for calculation of the flow regime transitions for a given flow condition.

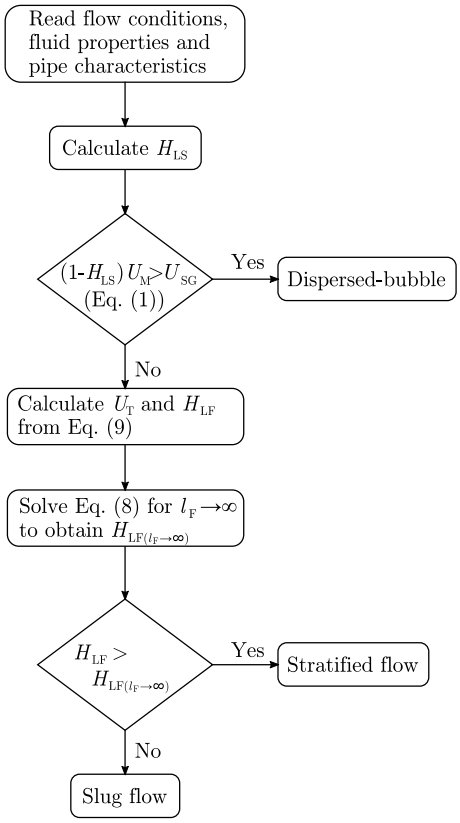

Figure 2: Flow regime transitions flow chart.

Figure 3 and Figure 4 show the performance of the proposed flow regime transition model for pipe inclinations of 0° and 4°, respectively. The transition from rolling waves to slug flow is reasonable well predicted by the model, with a slight under-prediction, for all flow combinations, annulus configurations, and pipe inclinations. This underprediction can be related to the interfacial shear stress approach used in our model, *i.e.* the model by Andritsos and Hanratty (1987) (as presented in Section 5.4) which does not consider high amplitude rolling waves and is based on low pressure data.

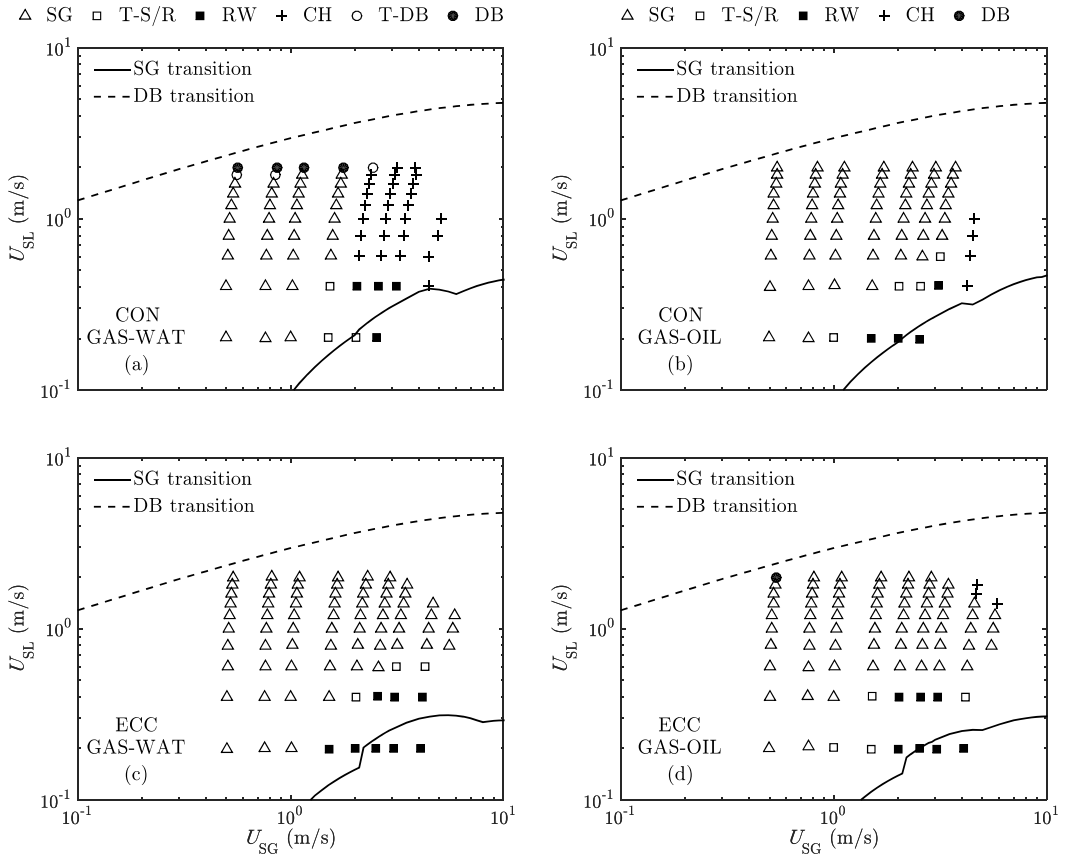

Figure 3: Flow regime transitions at a horizontal pipe for concentric (a and b) and fully eccentric annuli (c and d) for gas-water and gas-oil flow shown in the left and right column of panels, respectively (SG: slug flow; T-S/R: transition slug-rolling waves; RW: rolling waves; CH: churn flow; T-DB: transition to dispersed-bubble; DB: dispersed bubble flow).

Note that the transition slug to churn flow has not been included in this model. This would be of special interest for gas-water flows in a concentric annulus, based on the range of velocities studied in this work, and/or for gas-oil flows at high gas and liquid velocities. However, the early transition to churn flow in concentric gas-water flows (for a given U_{SL}) observed in the experiments might be attributed to the wetting properties of the pipe material for which further analysis must be performed to reach a reasonable conclusion.

The transition to dispersed-bubble flow is based on the slug liquid holdup which in turn is adopted from the Gregory *et al.* (1978) correlation. This results in a slight over-prediction for those cases where dispersed-bubble flow was observed, *i.e.* concentric gas-water (0°) and eccentric gas-oil (0° and 4°). The current test matrix (based on the maximum U_{SL} values studied) does not allow

us to reach a conclusive statement on the performance of this correlation as a criterion for the transition to dispersed-bubble flow.

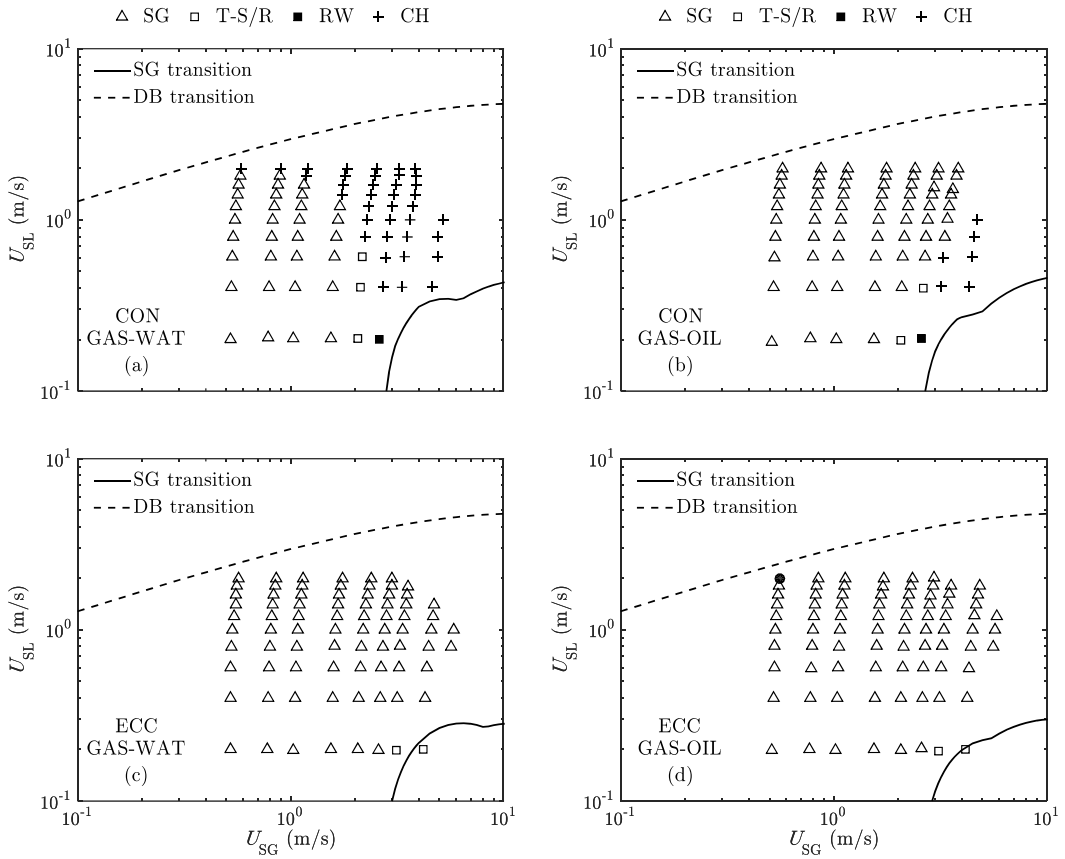

Figure 4: Flow regime transitions at a pipe inclination of 4° for concentric (a and b) and fully eccentric annuli (c and d) for gas-water and gas-oil flow shown in the left and right column of panels, respectively.

This model does not include the effect of liquid entrainment in the gas pocket for slug flow neither gas entrainment in the liquid film. No data is available on the entrainment fraction in annulus flows. Moreover, the closure relationships, such as the interfacial friction factor and the wetted perimeter are based on full pipe development adapted for the annulus geometry. These correlations need to be further validated or new expressions ought to be developed based on detailed experimental data. For example, X-ray tomography can be useful since it provides information on the distribution of the phases across the cross-section of the annulus pipe. This can

further be used to determine the shape of the film interface in the azimuthal direction and the wetted fraction.

Figure 5 shows comparisons of the predicted total liquid holdup, $H_L = H_{LS}(l_S/l_U)+H_{LF}(1-l_S/l_U)$, and the experimental data. Table 1 tabulates the absolute average relative error in percent, $e(\%)$,

$$e(\%) = \frac{1}{N}\sum_{i=1}^{N}\frac{\left|X_{\text{model,i}} - X_{\text{data,i}}\right|}{X_{\text{data,i}}} \times 100, \tag{10}$$

where variable of interest is denoted by X and N represent the number of samples of the statistical variable.

The absolute error of the model taking all flow regimes tested in this study is lower than 9% for any flow combinations, annulus configurations, and pipe inclinations. The best agreement between the model and measurement data is observed for slug flow. This can be attributed to the fact that origin of the model is based on the slug flow dynamics, thus, most of the phenomena that are encountered in this type of flows have been addressed. On the other hand, predictions for separated flows, *i.e.* rolling waves (RW) and transition slug to rolling waves (T-S/R), show the highest deviation from the measured liquid holdup data. This corresponds to the scattered prediction points at low H_L in Figure 5. This is not unexpected as the model does not account for the types of waves observed in the rolling wave regime. For churn flow, the no slippage criterion (*i.e.* $U_{G,slg} = U_{L,slg} = U_M$) might not be applicable due to the chaotic behaviour of the flow, for which the bubble velocity is lower than that for slug flow. This leads to the observed low accuracy of the total liquid holdup predictions for churn flow.

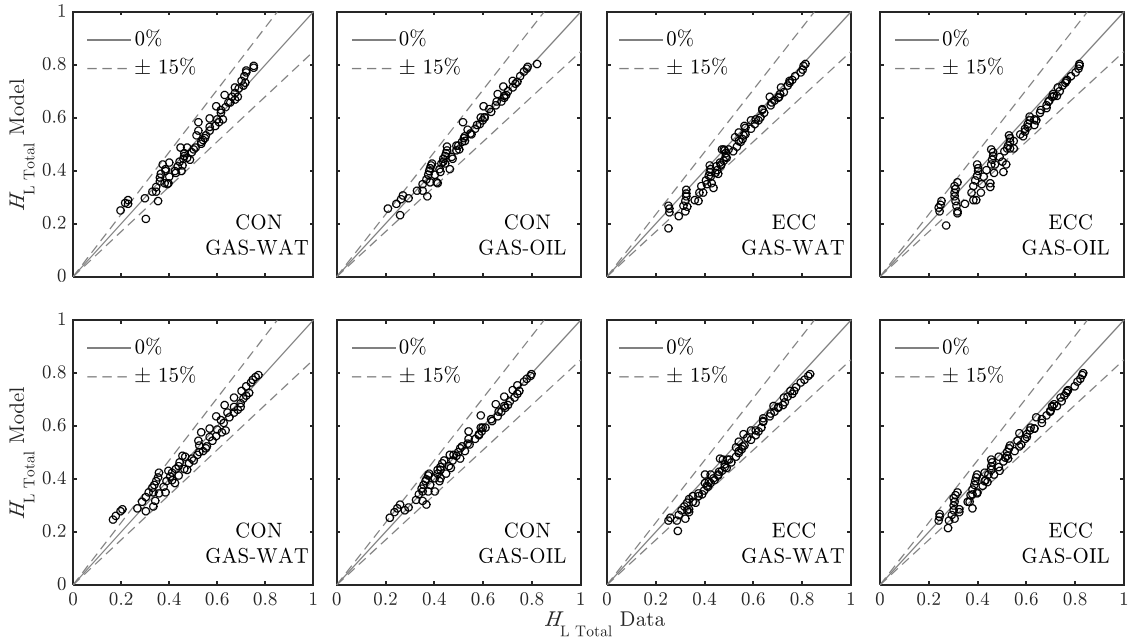

Figure 5: Total liquid holdup model performance with experiments for all data at θ = 0° (top row) and θ = 4° (bottom row).

Table 1: Total liquid holdup absolute average relative error for gas-water (G-W) and gas-oil (G-O) concentric and fully eccentric annuli (all corresponds to the entire data inclusive slug, churn and separated flows).

		e (%)			
θ	Regimes	Concentric		Eccentric	
		G-W	G-O	G-W	G-O
0°	All	6.4	4.3	7.0	8.6
	Slug	4.5	3.1	4.8	6.1
	Churn	7.7	14.4	–	12.4
	RW / T-S/R	12.7	8.5	20.9	23.5
4°	All	7.4	4.4	6.8	7.0
	Slug	3.8	3.6	6.3	6.7
	Churn	10.2	11.2	–	–
	RW / T-S/R	9.0	8.9	25.6	19.9

3 Modelling Pressure Gradient

The determination of the pressure gradient in the slug unit first involves the estimation of the slug and film characteristics. The liquid film (or Taylor bubble region) characteristics are obtained solving simultaneously the continuity equations (Eq. (3) to (6)) and the momentum equation (Eq.

(8)) for U_F, U_G, and H_{LF}. The slug liquid holdup, H_{LS}, and the Taylor bubble velocity, U_T, are estimated using closure relationships as described below. Note that the momentum exchange term in Eq. (8) requires calculation of the film length, l_F. This can be obtained from Eq. (7) with the slug length, l_S, estimated from a closure relation of Zhang *et al.* (2003a) (see Section 5 for further details). Finally, the slug unit pressure gradient is calculated as follows:

$$\left[\frac{\Delta P}{\Delta L}\right]_{l_U} = -\left[\frac{\tau_{slg} S_P}{A_P} + \rho_{slg} g \sin\theta\right]\frac{l_S}{l_U} - \left[\frac{\tau_G S_G + \tau_F S_F}{A_P} + \left(\rho_L H_{LF} + \rho_G (1 - H_{LF})\right) g \sin\theta\right]\left(1 - \frac{l_S}{l_U}\right), \quad (11)$$

where τ_{slg} is the slug shear stress (see Section 5.2), ρ_{slg} is the slug mixture density (see Section 5.3), S_P is the annulus pipe perimeter, $S_P = \pi(D_1+D_2)$, and the slug fraction, l_S/l_U, is calculated from Eq. (4) and (6).

Figure 6 and Table 2 show the performance of the model predictions for slug flow as compared with the measured total pressure gradient data. The good agreement between the model and the data is present across the cases covered in this study with an exception where we have observed our model under-predicting for when the gas-water flow through the concentric annulus. Based on our experimental observations in Ibarra *et al.* (2018) from the analysis of high-speed imaging and probability density function of the cross-sectional holdup data recorded by a broad-beam gamma densitometer, gas-water concentric annulus flows showed a non-consistent behaviour with irregular slug characteristics. As discussed in Ibarra *et al.* (2018), this can be attributed, in part, to the wettability of the pipe that has a larger effect in the concentric annulus configuration.

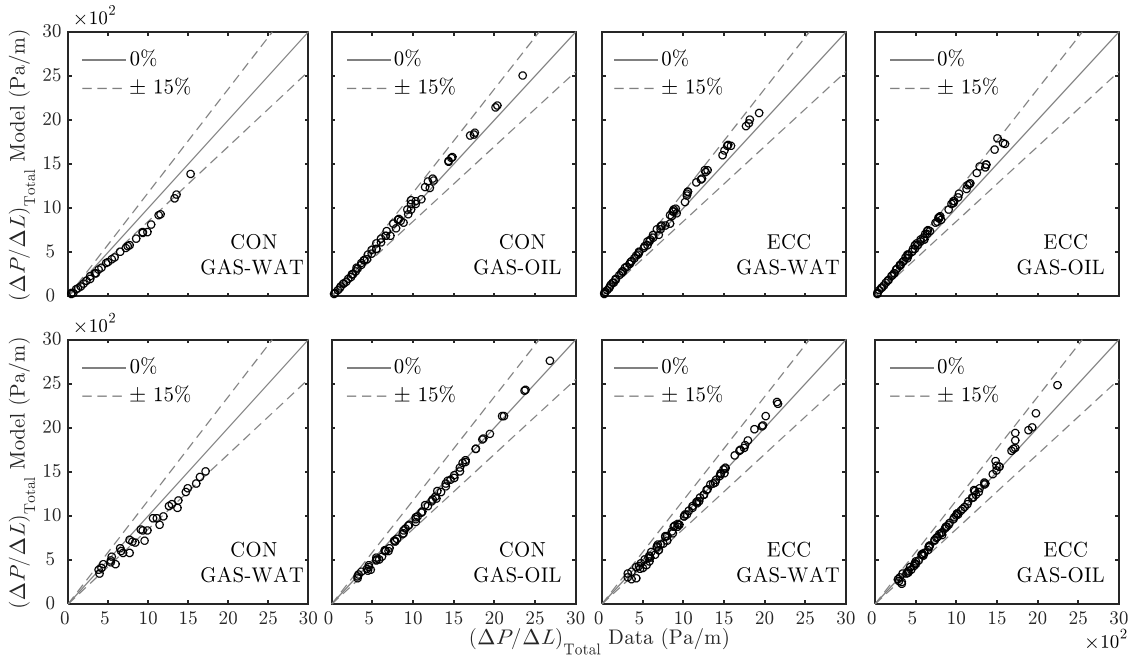

Figure 6: Total pressure gradient model performance with experiments for slug flow data at $\theta = 0°$ (top row) and $\theta = 4°$ (bottom row).

Table 2: Total pressure gradient absolute average relative error for gas-water (G-W) and gas-oil (G-O) slug flow in concentric and fully eccentric annuli.

θ	*e* (%)			
	Concentric		Eccentric	
	G-W	G-O	G-W	G-O
0°	22.9	4.7	9.7	12.7
4°	12.1	5.4	4.7	4.1

4 Model Sensitivity Analysis

A sensitivity analysis has been performed to determine which parameters have more weights on the model output (*i.e.* the total liquid holdup and/or the pressure gradient). The deviation of the model from a corresponding base case as a function of a specific parameter is calculated by varying an individual parameter while any others remain constant. The base case is defined as the case where all parameters remain constant (*i.e.* no variation) which are already presented in Figure 5 and Figure 6. The most dominant five parameters have been selected for the sensitivity analysis: U_{SG}, U_{SL}, D_1, D_2, and E, covering both inlet (superficial liquid and gas flow velocities) and boundary (pipe diameter ratio and eccentricity) conditions. Closures such as the slug bubble

velocity and shear stresses (*e.g.* τ_F, τ_G, τ_i) are recalculated accordingly based on the new value of the dominant parameters. These parameters are varied between ±5% of the original value used to compute the base case. The deviation of the model is calculated, for all flow conditions at each flow configuration, as the percentage average relative error of the results, *R*, to the base case,

$$\text{Deviation}(\%) = \frac{1}{N}\sum_{i=1}^{N}\frac{R_i - R_{\text{base,i}}}{R_{\text{base,i}}} \times 100, \tag{12}$$

where *N* is the number of flow conditions. Figure 7 and Figure 8 shows the average deviation for the total liquid holdup and pressure gradient, respectively, for gas-oil flows in concentric horizontal annulus.

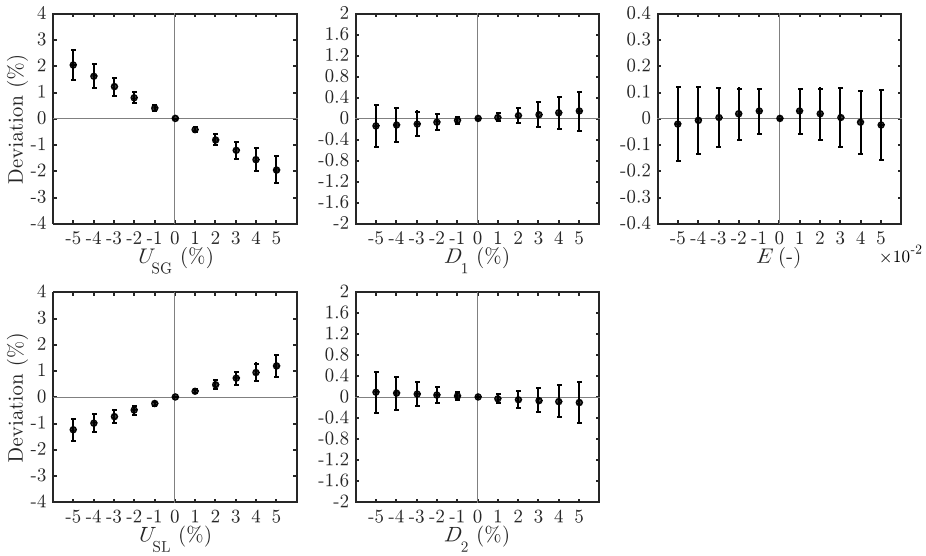

Figure 7: Model total liquid holdup sensitivity analysis for gas-oil flows in concentric horizontal annulus (error bars represent the standard deviation).

The sensitivity analysis indicates that variations of the annulus eccentricity have minor influence on the model output such as total liquid holdup and pressure gradient. This is also the case for the liquid holdup when we tested variations in the pipe diameter (D_1 or D_2). As expected, the total pressure gradient is found to be very much dependent on changes in D_1 or D_2 with deviations between −11% to 14% from the base case. This can further be analysed in terms of the pipe diameter ratio, *K*, where the pressure gradient decreases with decreasing *K* (negative deviation values for variations of $D_1(\%) > 0$ and $D_2(\%) < 0$ in Figure 8). The opposite behaviour is observed

for an increase in *K*, *i.e.* pressure gradient increases from the base case (positive deviation values for variations of $D_1(\%) < 0$ and $D_2(\%) > 0$ in Figure 8). Referring to the flow rates, variations in the superficial velocities result in deviations from the base total liquid holdup within ±3%. Deviations in the pressure gradient are slightly higher, especially for variations in U_{SL} as the liquid phase contributes more to the frictional losses than the gas phase.

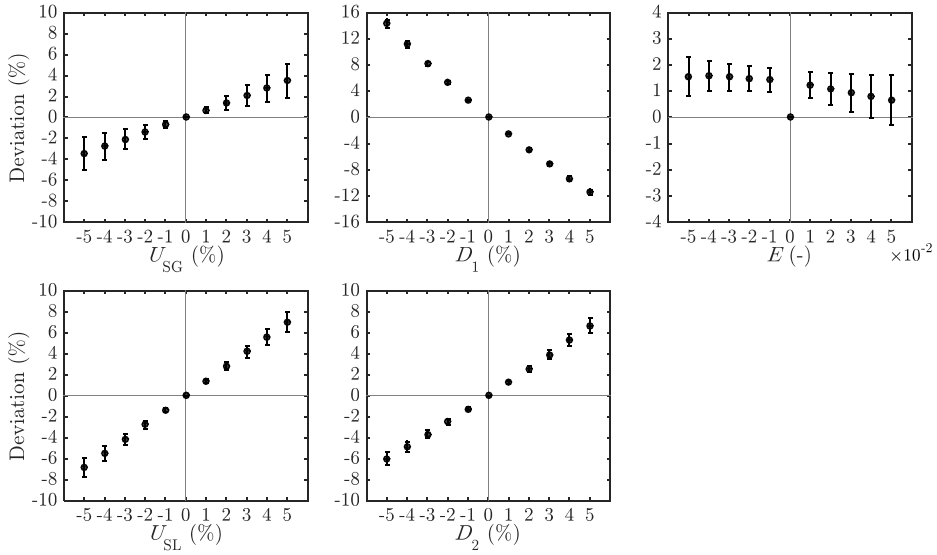

Figure 8: Model total pressure gradient sensitivity analysis for gas-oil flows in concentric horizontal annulus (error bars represent the standard deviation).

A sensitivity analysis was also performed on the coefficients for the wetted fraction and interfacial friction factor (see Section 5.1 and 5.4, respectively). These coefficients, *a* for the wetted fraction and b_1 and b_2 for the interfacial friction factor, were introduced to account for the annulus configuration. Results indicate that variations of each of these coefficients between ±10% of the base case have little effect on the total pressure gradient (see Figure 9) and insignificant influence on the total liquid holdup.

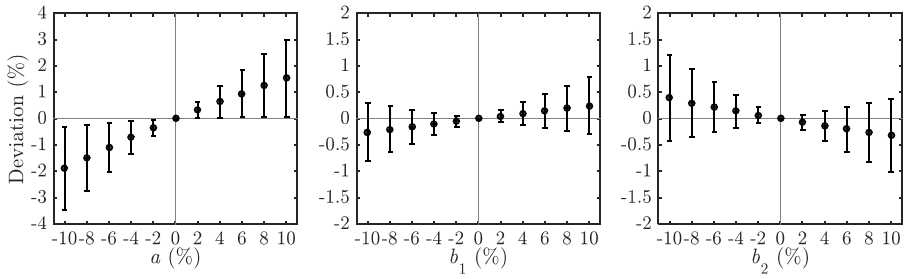

Figure 9: Sensitivity analysis of the predicted total pressure gradient with respect to wetted fraction and interfacial friction factor coefficient for gas-oil flows in concentric horizontal annulus (error bars represent the standard deviation).

5 Closure relationships

5.1 Geometrical considerations and wetted fraction

The wetted and interfacial perimeters in the film region are required in the calculation of the combined momentum equation and closure relationships. For a flat interface in the azimuthal direction, these perimeters are formulated as functions of the annulus diameter ratio, eccentricity, and the height of the liquid film, h_F, as shown Figure 10. In general, three cases result from the relative position of the film height with respect to the bottom of the inner pipe, $h^* = (D_1-D_2)/2+\delta$, where δ is the distance between pipe centres. Note that the degree of eccentricity, E, varies from −1 (fully eccentric at the bottom of the outer pipe) to 1 (fully eccentric at the top of the outer pipe).

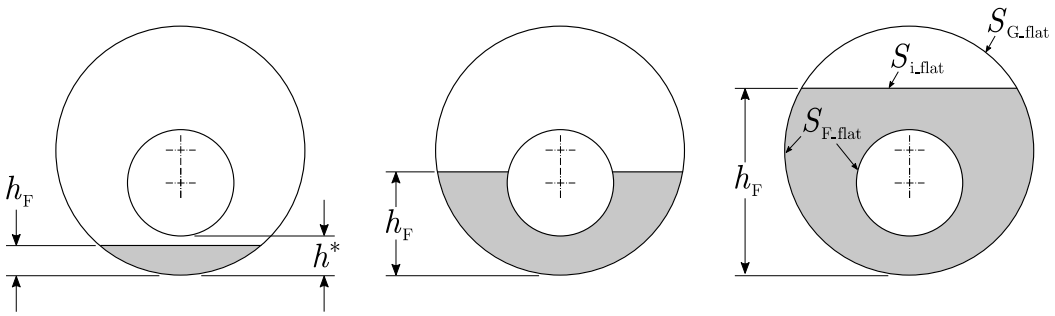

Figure 10: Film region geometrical parameters for a flat interface in the azimuthal direction.

The film and interfacial perimeters for a full pipe and a flat interface in the azimuthal direction can be calculated from

$$S_{\text{F\_flat\_FP}} = D\left[\pi - cos^{-1}\left(2\frac{h}{D} - 1\right)\right], \tag{13}$$

$$S_{\text{i\_flat\_FP}} = D\sqrt{1 - \left(2\frac{h}{D} - 1\right)^2}, \tag{14}$$

where h is the height of the liquid film and D is the diameter for a generic full pipe system. The selection of these variables (h and D) for an annulus pipe configuration is based on the three cases shown in Figure 10 and presented in Table 3.

Table 3: Film and interfacial perimeter in annulus for a flat interface ($S_{\text{F\_flat}}$ and $S_{\text{i\_flat}}$, respectively).

	$h_F \leq h^*$	$h^* < h_F < h^*+D_2$	$h_F \geq h^*+D_2$
Film	$S_{\text{F\_flat}} = S_{\text{F\_flat\_FP}}(h_F/D_1)$	$S_{\text{F\_flat}} = S_{\text{F\_flat\_FP}}(h_F/D_1)$ $+S_{\text{F\_flat\_FP}}((h_F - h^*)/D_2)$	$S_{\text{F\_flat}} = S_{\text{F\_flat\_FP}}(h_F/D_1)+\pi D_2$
Interfacial	$S_{\text{i\_flat}} = S_{\text{i\_flat\_FP}}(h_F/D_1)$	$S_{\text{i\_flat}} = S_{\text{i\_flat\_FP}}(h_F/D_1)$ $-S_{\text{i\_flat\_FP}}((h_F - h^*)/D_2)$	$S_{\text{i\_flat}} = S_{\text{i\_flat\_FP}}(h_F/D_1)$

The liquid film tends to wet the pipe as the gas velocity increases. The gas-liquid interface becomes concave until the liquid wets the entire pipe perimeter. We implement the wetted fraction, φ, correlation developed by Grolman and Fortuin (1997) for pipe flow in this work and modified it for annulus configurations as follows:

$$\varphi = \varphi_{\text{flat}}\left(\frac{\sigma_{\text{wat-gas}}}{\sigma}\right)^{0.15} + \frac{\rho_G}{(\rho_L - \rho_G)\cos\theta}\left(\frac{\rho_L U_{SL}^2 D_h}{\sigma}\right)^{0.25}\left(\frac{U_{SG}^2}{(1 - H_{LF})^2 g D_h}\right)^{0.8} a^{2.1}, \tag{15}$$

where φ_{flat} is the wetted fraction for a flat interface defined as $\varphi_{\text{flat}} = S_{\text{F\_flat}}/[\pi(D_1+D_2)]$ and a is a coefficient to account for the annulus configuration defined as $a = (1-K)(1-|E|/4)$. This coefficient, introduced in the velocity terms in the original Grolman and Fortuin (1997) expression, was developed from regression analysis of the pressure gradient and liquid holdup data as well as the performance of the transition between rolling waves and slug flow.

The final film and gas perimeter (*i.e.* S_F and S_G) is then calculated using the wetted fraction from Eq. (15), $S_F = \varphi S_P$ and $S_G = (1-\varphi)S_P$. This wetted fraction modifies the interfacial perimeter

which varies between a minimum value, S_{i_flat}, given for a flat interface in the azimuthal direction and a maximum value given for $\varphi = 1$ which corresponds to fully-wetted. However, there are cases where the minimum value of S_i is not given by a flat interface configuration and the evolution of the interfacial perimeter is not fully understood. In this work, we consider the interfacial perimeter as $S_i = S_{i\_flat}$ for all wetted fraction values in concentric and eccentric annulus flows.

5.2 Shear stress

Shear stresses for the slug, film region, gas region, and interface are defined as

$$\tau_{\mathrm{slg}} = \frac{1}{2} f_{\mathrm{slg}} \rho_{\mathrm{slg}} U_{\mathrm{M}}^2, \tag{16}$$

$$\tau_{\mathrm{F}} = \frac{1}{2} f_{\mathrm{F}} \rho_{\mathrm{F}} U_{\mathrm{F}}^2, \tag{17}$$

$$\tau_{\mathrm{G}} = \frac{1}{2} f_{\mathrm{G}} \rho_{\mathrm{G}} U_{\mathrm{G}}^2, \tag{18}$$

$$\tau_{\mathrm{i}} = \frac{1}{2} f_{\mathrm{i}} \rho_{\mathrm{G}} |U_{\mathrm{G}} - U_{\mathrm{F}}| (U_{\mathrm{G}} - U_{\mathrm{F}}), \tag{19}$$

where f is the friction factor.

5.3 Wall friction factor

For the stratified region, the film and gas Fanning friction factor at the wall for laminar flows is estimated as $f = 16/Re$ and for turbulent flows using the Zigrang and Sylvester (1982) correlation (see Eq. (A.2) for further details). The Reynolds numbers and hydraulic diameters for the friction factor calculation for the film and gas region are given as

$$Re_{\mathrm{F}} = \frac{\rho_{\mathrm{L}} U_{\mathrm{F}} D_{\mathrm{hF}}}{\mu_L}, \qquad D_{\mathrm{hF}} = \frac{4A_{\mathrm{F}}}{S_{\mathrm{F}}}; \tag{20}$$

$$Re_{\mathrm{G}} = \frac{\rho_{\mathrm{G}} U_{\mathrm{G}} D_{\mathrm{hG}}}{\mu_{\mathrm{G}}}, \qquad D_{\mathrm{hG}} = \frac{4A_{\mathrm{G}}}{S_{\mathrm{G}} + S_{\mathrm{i}}}. \tag{21}$$

In the liquid slug, the wall friction factor (Fanning), f_{slg}, is estimated using the approach presented in Appendix A for single-phase flows in concentric and eccentric annuli based on the mixture Reynolds number

$$Re_{\mathrm{slg}} = \frac{\rho_{\mathrm{slg}} U_{\mathrm{M}} D_{\mathrm{h}}}{\mu_{\mathrm{L}}}, \tag{22}$$

where the slug mixture density is defined as

$$\rho_{\mathrm{slg}} = \rho_{\mathrm{L}} H_{\mathrm{LS}} + \rho_{\mathrm{G}}(1 - H_{\mathrm{LS}}). \tag{23}$$

For the transitional region (1700 < *Re* < 3000), the wall/slug friction factor is interpolated between the laminar and turbulent values.

5.4 Interfacial friction factor

Interfacial friction factor, f_{i}, is needed for computing interfacial shear stress. Taitel and Dukler (1976) suggested that $f_{\mathrm{i}} = f_{\mathrm{G}}$ for stratified-smooth flows. Cohen and Hanratty (1968) proposed a value of $f_{\mathrm{i}} = 0.0142$ for stratified-wavy flows with small amplitude waves. In this work, we use a modified Andritsos and Hanratty (1987) correlation where the term h_{F}/D has been replaced by the holdup in the liquid film region, H_{LF}, and coefficients adapted for the annulus configuration as follows:

$$\begin{aligned} f_{\mathrm{i}} &= f_{\mathrm{G}}, && U_{\mathrm{SG}} < U_{\mathrm{SG,t}}; \\ f_{\mathrm{i}} &= f_{\mathrm{G}}\left[1 + b_1\sqrt{H_{\mathrm{LF}}}\left(\frac{U_{\mathrm{SG}}}{U_{\mathrm{SG,t}}} - 1\right)\right], && U_{\mathrm{SG}} \geq U_{\mathrm{SG,t}}; \end{aligned} \tag{24}$$

where the critical gas velocity, $U_{\mathrm{SG,t}}$, is defined as

$$U_{\mathrm{SG,t}} = b_2\sqrt{\frac{\rho_{\mathrm{G,ATM}}}{\rho_{\mathrm{G}}}}. \tag{25}$$

Here, we modified coefficients b_1 and b_2 (given in SI units, m/s) to account for the annulus configuration. In our formulation, $b_1 = 15/[(1-K/4)(1-|E|/4)]$ and $b_2 = 5(1-K)$.

Tzotzi and Andritsos (2013) modified the model by Andritsos and Hanratty (1987) by categorising stratified flow into three sub-regimes: (i) smooth region, (ii) two-dimensional (2-D) wave region with small amplitude, short wavelength, and (iii) a wavy region with large amplitude, irregular waves, called Kelvin-Helmholtz (K-H) waves. However, it was found that this model

results in a larger under-prediction of the slug/rolling waves transition than our proposed approach (adapted for flow in annuli).

5.5 Slug bubble velocity

The translational or Taylor bubble velocity in slug flow is predicted using the approach presented by Ibarra and Nossen (2018) for flow in annuli. The bubble velocity can be modelled using the Nicklin *et al.* (1962) expression based on drift flux,

$$U_{\mathrm{T}} = C_{\mathrm{O}} U_{\mathrm{M}} + U_{\mathrm{d}}, \tag{26}$$

where C_{O} is the distribution parameter and U_{d} is the drift velocity of the bubble.

For mixture Froude numbers, Fr_{M}, lower than a critical value, $Fr_{\mathrm{M}} < Fr_{\mathrm{M,C}} \approx 3.3$, where

$$Fr_{\mathrm{M}} = \frac{U_{\mathrm{M}}}{\sqrt{g D_{\mathrm{h}} (1 - \rho_{\mathrm{G}}/\rho_{\mathrm{L}})}}, \tag{27}$$

C_{O} and U_{d} are estimated using the Smith *et al.* (2015) development as follows:

$$C_{\mathrm{O}} = \max\left(1.05, C_{\mathrm{O,f}}\right) + 0.15 \sin^2\theta, \tag{28}$$

where $C_{\mathrm{O,f}}$ is based on the Reynolds number as developed by Nuland (1998)

$$\begin{aligned} C_{\mathrm{O,f}} &= C_{\mathrm{O,lam}} = 2, && Re \leq 1700; \\ C_{\mathrm{O,f}} &= C_{\mathrm{O,turb}} = \frac{(n+1)(2n+1)}{2n^2}, && Re \geq 3000; \\ C_{\mathrm{O,f}} &= w C_{\mathrm{O,turb}} + (1-w) C_{\mathrm{O,lam}}, && 1700 < Re < 3000; \end{aligned} \tag{29}$$

with

$$w = \frac{Re_{\mathrm{slg}} - 1700}{3000 - 1700}. \tag{30}$$

The factor n represents the inverse exponent in the power law velocity profile for turbulent flow based on the von Karman constant ($\kappa = 0.41$)

$$n = \kappa \sqrt{2/f_{\mathrm{slg}}}. \tag{31}$$

The drift velocity is estimated as

$$U_{\mathrm{d}} = (Fr_{\mathrm{v}} \sin\theta + Fr_{\mathrm{h}} \cos\theta)\sqrt{gD_{\mathrm{h}}(1-\rho_{\mathrm{G}}/\rho_{\mathrm{L}})}, \tag{32}$$

where $Fr_{\mathrm{v}} = 0.351$ and $Fr_{\mathrm{h}} = 0.542$.

For $Fr_{\mathrm{M}} \geq Fr_{\mathrm{M,C}}$, the distribution parameter and the drift velocity are a function of the annulus eccentricity,

$$C_{\mathrm{O}} = 1.38\left(1 - \frac{|E|}{18}\right), \tag{33}$$

$$U_{\mathrm{d}} = 0.25(|E|)\sqrt{gD_{\mathrm{h}}(1-\rho_{\mathrm{G}}/\rho_{\mathrm{L}})}. \tag{34}$$

5.6 Slug length

The slug length can be estimated using the expression proposed by Zhang *et al.* (2003a) using the hydraulic diameter of the annulus pipe

$$l_{\mathrm{S}} = (32\cos^2\theta + 16\sin^2\theta)D_{\mathrm{h}}. \tag{35}$$

6 Conclusions

A model to predict the flow regime transitions, liquid holdup and pressure gradient for horizontal and low-inclination two-phase flow in annuli has been developed. The model is based on slug flow dynamics where the transition to dispersed-bubble is given by the hypothesis that the gas in the liquid slug is dispersed as bubbles and the transition to slug flow is defined using the minimum slip criterion. The experimental data (average holdup and pressure gradient) of Ibarra *et al.* (2018) are used to test the model showing good agreements for both concentric and fully eccentric annuli with the exception of pressure gradient predictions in horizontal concentric gas-water flow where an under-prediction of about 23% of the absolute average relative error is observed. This might be attributed to the irregular slug characteristics which dominate the flow regime map for the flow conditions studied.

The performance of the closure relationships directly affects the model predictions. For example, the calculation of the total liquid holdup in the slug unit is based on the slug liquid holdup (see Taitel and Barnea, 1990; for slug flow and Soedarmo *et al.*, 2018; for churn flow). In our work,

the Gregory *et al.* (1978) correlation, which was originally developed for full pipe flow, has been used to calculate the holdup in the liquid slug. The validity and applicability range of this correlation must therefore be validated with detailed data for flow in annuli. This is also the case of closures, such as, the interfacial friction factor, the wetted fraction, and the slug length, which have been modified to account for the annulus geometry, *i.e.* pipe diameter ratio and eccentricity. Finally, it is recommended to perform studies on the bubble or structure velocity in churn flows in annuli as this directly affects the calculation of the total liquid holdup in the slug unit.

Acknowledgements

This work has been performed thanks to the funding of the Research Council of Norway through the PETROMAKS2 programme. The authors would like to express their gratitude to Joar Amundsen and Hans-Gunnar Sleipnæs for their assistance during the experimental campaign.

Appendix A. Single-phase friction factor

The friction factor in concentric and eccentric single-phase annulus flows can be estimated using the Caetano *et al.* (1992a) model, which was modified and validated by Ibarra and Nossen (2018). In this model, a geometry parameter, G, modifies the full pipe friction factor, f_{FP}, as follows

$$f_{\mathrm{CON/ECC}} = f_{\mathrm{FP}}\left(G_{\mathrm{CON/ECC}}\right)^{c}, \tag{A.1}$$

where the full pipe Fanning friction factor for laminar flows is estimated as $f_{\mathrm{FP}} = 16/Re$. For turbulent flows the Zigrang and Sylvester (1982) correlation can be used

$$\frac{1}{\sqrt{f_{\mathrm{FP}}}} = -4\log\left\{\frac{\epsilon}{3.7D_{\mathrm{h}}} - \frac{5.02}{Re}\log\left[\frac{\epsilon}{3.7D_{\mathrm{h}}} - \frac{5.02}{Re}\log\left(\frac{\epsilon}{3.7D_{\mathrm{h}}} + \frac{13}{Re}\right)\right]\right\}, \tag{A.2}$$

where ϵ is the roughness of the pipe and the Reynolds number is defined as $Re = \rho U D_{\mathrm{h}}/\mu$.

For concentric annulus, the geometry parameter is

$$G_{\mathrm{CON}} = K_0 \frac{(1-K)^2}{\dfrac{1-K^4}{1-K^2} - \dfrac{1-K^2}{\ln(1/K)}}, \tag{A.3}$$

where the empirical correction factor K_0 has been introduced to obtain a better performance for a wider range of the diameter ratio and is given by

$$K_0 = \max(0.68, K_1), \tag{A.4}$$

$$K_1 = 1 - |0.56 - K|. \tag{A.5}$$

For eccentric annulus, the geometry parameter is

$$G_{\mathrm{ECC}} = \frac{(1-K)^2(1-K^2)}{4\Phi \sinh^4 \eta_0}, \tag{A.6}$$

where

$$\cosh \eta_0 = \frac{K(1-E^2)+(1+E^2)}{2E}, \tag{A.7}$$

$$\cosh \eta_1 = \frac{K(1+E^2)+(1-E^2)}{2KE}, \tag{A.8}$$

$$\Phi = (\coth \eta_1 - \coth \eta_0)^2 \left[\frac{1}{\eta_0 - \eta_1} - 2\sum_{j=1}^{\infty} \frac{2j}{e^{2j\eta_1} - e^{2j\eta_0}}\right] + \frac{1}{4}\left(\frac{1}{\sinh^4 \eta_0} - \frac{1}{\sinh^4 \eta_1}\right). \tag{A.9}$$

Finally, the exponent c for laminar flows is equal to unity and for turbulent flows

$$c = 0.45e^{-(Re-3000)/10^6}. \tag{A.10}$$

References

Andritsos, N., Hanratty, T.J. (1987) Influence of interfacial waves in stratified gas-liquid flows. AIChE, 33, 444-454.

Barnea, D., Brauner, N. (1985) Holdup of the liquid slug in two-phase intermittent flow. Int. J. Multiph. Flow, 11, 43-49.

Caetano, E.F., Shoham, O., Brill, J.P. (1992a) Upward vertical two-phase flow through an annulus-Part I: Single-phase friction factor, Taylor bubble rise velocity, and flow pattern prediction. J. Energy Resour. Technol., 114(1), 1-13.

Caetano, E.F., Shoham, O., Brill, J.P. (1992b) Upward vertical two-phase flow through an annulus-Part II: Modeling bubble, slug, and annular flow. J. Energy Resour. Technol., 114(1), 1-17.

Cohen, S.L., Hanratty, T.J. (1968) Effects of waves at a gas-liquid interface on a turbulent air flow. J. Fluid Mech., 31, 467.

Das, G., Das, P.K., Purohit, N.K., Mitras, A.K. (1999) Flow pattern transition during gas liquid upflow through vertical concentric annuli-Part II: mechanistic models. J. Fluids Eng., 121, 902-907.

Gregory, G.A., Nicholson, M.K., Aziz, K. (1978) Correlation of the liquid volume fraction in the slug for horizontal gas-liquid slug flow. Int. J. Multiph. Flow, 4, 33-39.

Grolman, E., Fortuin, J.M.H. (1997) Gas-liquid flow in slightly inclined pipes. Chem. Eng. Sci., 52(24), 4461-4471.

Hasan, A.R., Kabir, C.S. (1992) Two-phase flow in vertical and inclined annuli. Int. J. Multiph. Flow, 18(2), 279-293.

Ibarra, R., Nossen, J. (2018) Bubble velocity in horizontal and low-inclination upward slug flow in concentric and fully eccentric annuli. Chem. Eng. Sci., 192, 774-787.

Ibarra, R., Nossen, J., Tutkun, M. (2018) Two-phase gas-liquid flow in concentric and fully eccentric annuli. Part I: Flow patterns, holdup, slip ratio and pressure gradient. Submitted to Chem. Eng. Sci.

Julia, J.E., Hibiki, T. (2011) Flow regime transition criteria for two-phase flow in a vertical annulus. Int. J. Heat Fluid Flow, 32, 993-1004.

Kelessidis, V.C., Dukler, A.E. (1989) Modeling flow pattern transitions for upward gas-liquid flow in vertical concentric and eccentric annuli. Int. J. Multiph. Flow, 15(2), 173-191.

Mishima, K., Ishii, M. (1984) Flow regime transition criteria for upward two-phase flow in vertical tubes. Int. J. Heat Mass Trans., 27, 723-737.

Nicklin, D.J., Wilkes, J.O., Davidson, J.F. (1962) Two-phase flow in vertical tubes. Trans. Inst. Chem. Eng., 40, 61-68.

Nuland, S. (1998) Bubble front velocity in horizontal slug flow with viscous Newtonian, shear thinning and Bingham fluids. 3rd International Conference on Multiphase Flow, June 8-12. Lyon, France.

Smith, I.E., Nossen, J., Kjølaas, J., Lund, B. (2015) Development of a steady-state point model for prediction of gas/oil and water/oil pipe flow. J. Disper. Sci. Technol., 36(10), 1394-1406.

Soedarmo, A., Fan, Y., Pereyra, E., Sarica, C. (2018) A unit cell model for gas-liquid pseudo-slug flow in pipes. J. Nat. Gas Sci. Eng., 60, 125-143.

Sun, X., Kuran, S., Ishii, M. (2004) Cap bubbly-to-slug flow regime transition in a vertical annulus. Exp. Fluids, 37, 458-464.

Taitel, Y., Barnea, D. (1990) Two-phase slug flow. Advances in Heat Transfer, 20, 83-132.

Taitel, Y., Barnea, D., Dukler, A.E. (1980) Modelling flow pattern transitions for steady upward gas-liquid flow in vertical tubes. AIChE J., 26, 345-354.

Taitel, Y., Dukler, A.E. (1976) A model for predicting flow regime transitions in horizontal and near horizontal gas-liquid flow. AIChE J., 22(1), 47-55.

Tzotzi, C., Andritsos, N. (2013) Interfacial shear stress in wavy stratified gas-liquid flow in horizontal pipes. Int. J. Multiph. Flow, 54, 43-54.

Yu, T.T., Zhang, H.Q., Li, M.X., Sarica, C. (2010) A mechanistic model for gas/liquid flow in upward vertical annuli. SPE Prod. Oper., 25(3), 285-295.

Zhang, H.Q., Wang, Q., Sarica, C., Brill, J.P. (2003a) A unified mechanistic model for slug liquid holdup and transition between slug and dispersed bubble flows. Int. J. Multiph. Flow, 29, 97-107.

Zhang, H.Q., Wang, Q., Sarica, C., Brill, J.P. (2003b) Unified model for gas-liquid pipe flow via slug dynamics - Part 1: Model development. J. Energy Resour. Technol., 125, 266-273.

Zigrang, D.J., Sylvester, N.D. (1982) Explicit approximations to the solution of Colebrook's friction factor equation. AIChE, 28(3), 514-515.